DOI: 10.1002/ejic.200800383

Crystal Packing in Di-(μ-OH)-*ortho*-palladated Complexes – A DFT Insight into the Molecular Structure and Solid-State Interactions

Jose Pérez,*[a] Arturo Espinosa,*[b] Jose M. Galiana,[a] Eduardo Pérez,[a] Jose L. Serrano,[a] Aurelio Cabeza,[c] and Miguel A. G. Aranda[c]

Keywords: Palladium complexes / X-ray powder diffraction / Density functional calculations / Hydrogen bonds / Stacking interactions

The crystal structures of [Pd(μ-OH)(C^N)]$_2$ [C^N = phpy = 2-(2-pyridyl)phenyl (**1**), C^N = bzq = 7,8-benzoquinolin-10-yl (**2**)] have been elucidated by ab initio X-ray powder diffraction methodology with monochromatic Cu-$K_{\alpha 1}$ radiation. The crystal structures have been refined by the Rietveld method. Both complexes exhibit a planar conformation in the solid state (which is the most frequent for this type of compounds as found in the Cambridge Structural Database). In compound **1**, three molecules are stacked in an overlapping parallel orientation. DFT calculations reveal that hydrogen bonds and Pd···Pd interactions are the reasons for the stability of this "trimer".

Introduction

The understanding and utilization of all noncovalent interactions including π–π stacking is of fundamental importance for the further development of (inorganic) supramolecular chemistry and the fine tuning and prediction of crystal structures.[1–6]

The order of stability in the interaction of two π systems has been found to be π-deficient–π-deficient > π-deficient–π-rich > π-rich–π-rich.[7] In the systems under study, a nitrogen heteroatom within a six-membered ring introduces an electron-withdrawing perturbation. Pyridine, bipyridines, and other aromatic nitrogen heterocycles are known as electron-poor ring systems (relatively inert to electrophilic attack and with enhanced reactivity towards nucleophiles). A metal that is coordinated to a nitrogen heteroatom will further increase the electron-withdrawing effect through its positive charge. Hence, six-membered aromatic nitrogen heterocycles should, in principle, be well suited for π–π interactions because of their low π-electron density. Stacking in complexes containing this type of ligands does not show a perfect face-to-face alignment of the atoms but usually exhibits an offset or slipped packing.[6]

In the structural description of metal complexes with these ligands, π–π stacking is an increasingly noted feature. Furthermore, it is not just a structural phenomenon, since it has also been correlated with the solid-state luminescence properties of some metal complexes, notably with platinum[8,9] but also with gold[10] and other metals.[11]

The synthetic value of palladium(II) and platinum(II) di-(μ-OH) complexes is a subject of current study.[12] In this sense, during the last years we have also been studying the usefulness of dinuclear hydroxido complexes of palladium, some of them with a cyclometalated backbone, in the preparation of a wide variety of new compounds by means of a simple acid–base reaction.[13] In this article we focus our attention on the structural solid state of some of these precursors (Scheme 1) by a combination of X-ray diffraction, DFT calculations, and data retrieved from the Cambridge Structural Database (CSD).

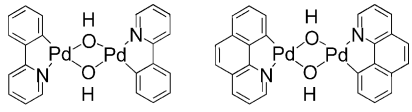

Scheme 1.

Results and Discussion

Structure Determination by Powder X-ray Diffractometry

Data Reduction and Indexing

The peak positions were identified by using a derivative-based algorithm that is implemented in the peak search util-

[a] Departamento de Ingeniería Minera, Geológica y Cartográfica, Área de Química Inorgánica, Universidad Politécnica de Cartagena,
30203 Cartagena (Murcia), Spain
[b] Departamento de Química Orgánica, Universidad de Murcia, 30071 Murcia, Spain
[c] Departamento de Química Inorgánica, Universidad de Málaga, Campus Teatinos,
29071 Málaga, Spain
Supporting information for this article is available on the WWW under http://www.eurjic.org or from the author.

ity of the WINPLOTR software package.[14] The indexing was carried out with the commonest indexing programs: ITO, TREOR90, DICVOL, KOHL, TAUP, FJZN, and LZON. The best solution for **1**, obtained with DICVOL06, was a monoclinic cell with a = 15.983(5) Å, b = 16.184(9) Å, c = 10.963(3) Å, β = 92.15(3)°, V = 2833.86(3) Å^3, and $M(20)$ = 30.3. For **2**, the best solution, obtained with DICVOL106, was a monoclinic cell with a = 17.712(3) Å, b = 3.714(1) Å, c = 15.205(3) Å, β = 92.49(2)°, V = 999 Å^3, and $M(20)$ = 33.7. By examining the data with CHECKCELL,[15] the space group was unambiguously found to be $P2_1/n$ for **1** and $P2_1/c$ for **2**, or the possible subgroups. From the cell volume, we deduced the presence within the asymmetric unit of 1.5 molecules in case **1** and a half molecule in case **2**.[16]

To assess the goodness of the space group and the choice of the cell and to estimate the shape and width of the Bragg reflections as well as the instrumental shifts, we also performed the Le Bail fit[17] implemented as the profile-matching option in the FULLPROF program.[18] This fitting procedure, which makes no reference to any structure model, was conducted by describing the peak shape with a pseudo-Voigt function, with the Berar–Baldinozzi asymmetry correction.[19] In complex **1**, the background was corrected by a linear interpolation between 52 points regularly distributed along the pattern. The final residuals were R_p = 5.83, R_{wp} = 8.61, $R_{exp.}$ = 3.45, and χ^2 = 6.22. In complex **2**, the background was corrected by a linear interpolation between 60 points regularly distributed along the pattern. The final residuals were R_p = 5.20, R_{wp} = 6.96, $R_{exp.}$ = 3.26, and χ^2 = 4.56. The low values of these residuals confirm the validity of the space group and cell found.

Structure Solution

In complex **1** a first approximation to the crystal structure was obtained by Monte Carlo methods, using the parallel tempering algorithm implemented in the FOX software package.[20] To that end, the metal atoms and aromatic ligands were treated as independent blocks, and the ligands were treated as rigid bodies (bond lengths and angles fixed). It was necessary also to refine the preferred orientation along the –101 reflection with the March–Dollase function.[21,22] After 17000000 movements, the weighted residual was R_{wp} = 0.24. We observed that the ligands and Pd atoms converged to nearly coplanar positions, with distances Pd–C and Pd–N close to the bond length (ca. 2 Å).

In complex **2** the Le Bail fit yielded 1026 reflections that allowed obtaining by direct methods using the Sir2004 software[23] the positions of palladium atoms in the cell and atoms bonded to palladium. To locate the 7,8-benzoquinoline-1,10-diyl ligand it was necessary to use the Monte Carlo method, which, after 2000000 movements, yielded a weighted residual of R_{wp} = 0.26.

Rietveld Refinement

The atomic coordinates obtained by Monte Carlo methods were used to initialize the Rietveld refinements, which were performed by using the FULLPROF program.[18] In a first step we refined the scale factor, the instrumental shifts (zero-point 2θ shift, and systematic shifts depending on the transparency and off-centering of the sample), the background, the Debye–Waller global parameter, and the cell parameters, as well as the shape, width, and asymmetry of the Bragg reflections assumed to have pseudo-Voigtian form, while fixing all atomic coordinates. The hydrogen atoms were added at the theoretical positions except the hydroxyl hydrogen atoms that could not be positioned properly. In a second Rietveld refinement stage, soft constrains were imposed on the atom–atom distances for the palladium and oxygen atoms, whereas the *ortho*-metalated ligands were rigidly refined. A global Biso was used, in complex **2** it was possible to refine an individual Biso for the Pd atom. The refining of preferred orientation along the –101 and –102 reflections for **1** and **2**, respectively, improved the refinement significantly. The modified March function implemented in FULLPROF was employed for this purpose. The plot output from the Rietveld analysis is shown in Figure 1.

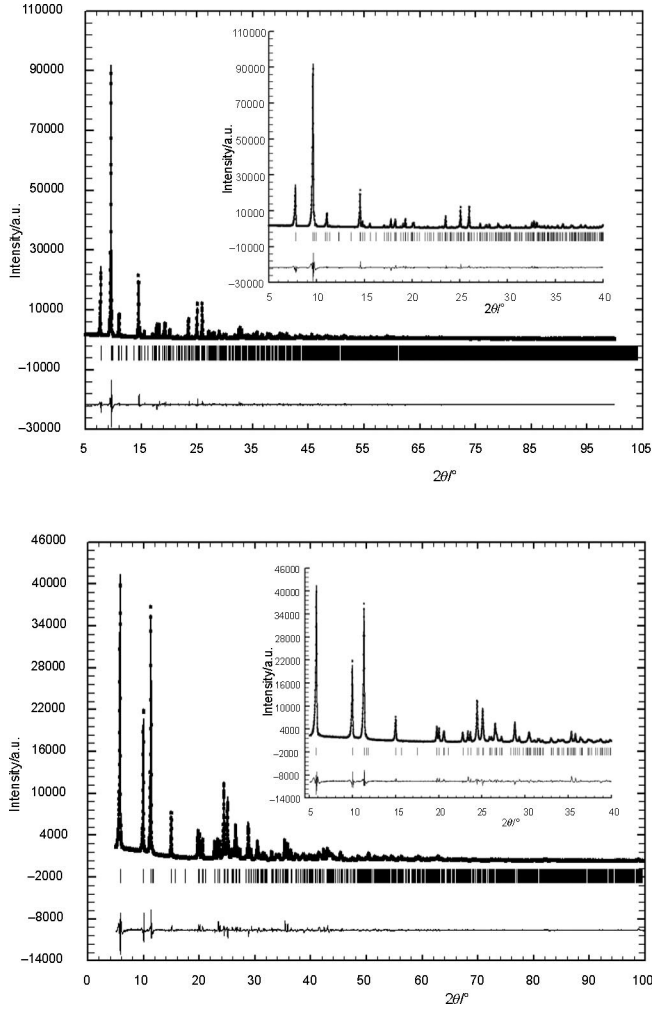

Figure 1. Plot output from the Rietveld analysis of the X-ray diffraction pattern corresponding to the complexes [{Pd(μ-OH)(phpy)}$_2$] (**1**) (top) and [{Pd(μ-OH)(bzq)}$_2$] (**2**) (bottom). The dots are the experimental X-ray diffraction data, the solid line is the calculated pattern, and the residuals are plotted as the line at the bottom.

The crystal structure of complex **1** has been elucidated previously by some of us by using Cu-$K_{\alpha 1,2}$ radiation;[24] the use of strictly monochromatic radiation improves the structural elucidation and yields more reliable information about the relative positions of molecules in the packing. Molecular structures of complexes **1** and **2** are shown in Figure 2.

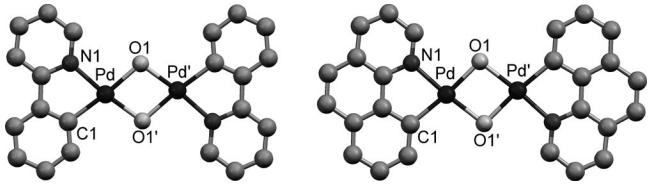

Figure 2. Molecular structure of complex **1** (left) and complex **2** (right). Relevant distances in **1** (mean values in Å): Pd–N 2.067, Pd–C 2.020, Pd–O 2.032, Pd–Pd′ 3.179. Relevant distances in **2** (in Å): Pd–N 2.066, Pd–C 2.056, Pd–O 2.081, Pd–Pd′ 3.142.

The most relevant feature in crystal packing of complexes **1** and **2** is that molecules appear stacked in a parallel orientation, but there is a significant difference between the two structures: the parallel stacking in **1** extends over discrete units comprising three molecules, while in **2** it extends to the complete crystal (Figure 3).

Conformational Preferences and Crystal Packing in Di-(μ-OH) Complexes

A survey in the CSD revealed the existence of sixteen dinuclear Pd complexes bridged by two OH groups. Their reference codes and selected geometrical parameters are listed in Table 2. The average value of the Pd–O distance calculated for these complexes is 2.064 Å. The O–Pd–O and Pd–O–Pd angles vary in narrow ranges and have average values of 79.55° and 97.82°, respectively. A relevant conformational parameter in these complexes is the Pd···Pd distance, which is observed to range between 2.97 and 3.20 Å with a mean value of 3.11 Å. Complexes **1** and **2** show values within that range.

As can be seen in Table 1, the planar conformation is the most frequent one in di-(μ-OH) palladium complexes. Furthermore, it is the most frequent conformation in di-(μ-OH) square-planar complexes in group 10: the survey in the CSD yielded 28 platinum complexes (21 of them having a planar conformation) and 6 nickel complexes (4 of them having a planar conformation). Structures reported in this paper also have a planar conformation, in agreement with the aforementioned general trend in di-(μ-OH) square-planar complexes.

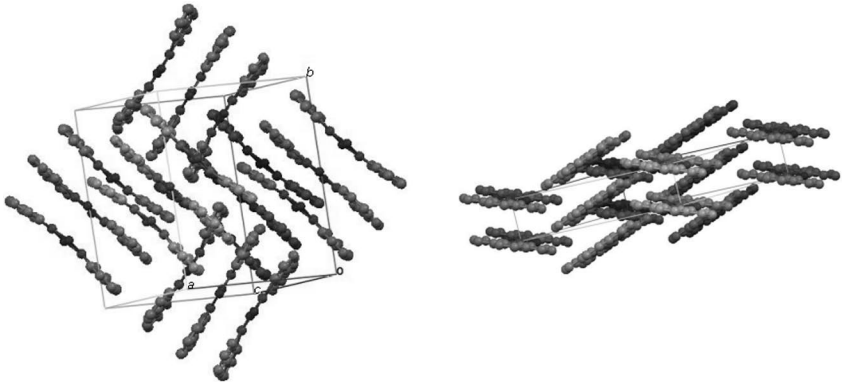

Figure 3. Crystal structures of **1** (left) and **2** (right).

Table 1. Relevant geometrical parameters in complexes containing a $\{Pd(\mu\text{-}OH)\}_2$ core.

Reference code	Mean Pd–O /Å	Mean O–Pd–O /°	Mean Pd–O–Pd /°	Pd···Pd /Å	Pd–O–Pd–O /°
DEGKUW[25a]	2.023(2)	80.38(7)	99.30(5)	3.083	5.92
FACHEX[25b]	2.06(4)	80.39(0)	99.61(0)	3.141	0
IXOMOX[25c]	2.072(1)	80.85(4)	98.77(5)	3.145	–6.60
JIHJIT[25d]	2.08(1)	77.04(8)	96.3(1)	3.095	–27.13
KEFLIQ[25e]	2.09(3)	79.8(2)	99(2)	3.170	–11.90
LANBOR[25f]	2.09(2)	76.8(2)	90.8(6)	2.981	35.75
MALDAE[25g]	2.015(9)	76.58(9)	95.5(6)	2.984	–29.74
MARCUD[25h]	2.005(0)	82.34(0)	97.66(0)	3.018	0
NACVAP[25i]	2.08(2)	78.5(5)	92.9(7)	3.016	31.25
QEJCIS[25j]	2.11(2)	81.5(9)	98.5(9)	3.199	0
QIYWOK[25k]	2.017(2)	81.70(0)	98.30(0)	3.051	0
SOGHOL[25l]	2.073(6)	81.21(0)	98.79(0)	3.147	–0.03
ULINAE[25m]	2.023(1)	81.95(2)	94.45(1)	2.971	20.14
YIBMAY[25n]	2.069(9)	79.73(4)	98.6(6)	3.138	13.92
YUNBOY[25o]	2.079(3)	80.19(0)	99.81(0)	3.179	0.03
XAYGOU[25p]	2.034(6)	80.38(0)	99.62(0)	3.108	0
Complex **1**	2.03(3)	77(1)	103(2)	3.179(10)	0.57
Complex **2**	2.08(2)	82.0(9)	98.05(6)	3.142	0

In order to compare the crystal packing in the structures reported herein with those in similar compounds in the CSD, planar molecules (H atoms were not considered for planarity) containing the $\{M(\mu\text{-}OH)\}_2$ core were analyzed. In all cases, stacking of parallel molecules was observed in the crystal structure. With the aim of characterizing the relative position of the molecules, the following two parameters were employed (Figure 4): (i) the distance between planes, C_P, calculated as the distance from the centroid of the core $\{M(\mu\text{-}OH)\}_2$ to the mean plane defined by the second molecule; (ii) the deviation angle, ϕ, calculated as the angle formed by vector **C_P** and vector **C_C**, where vector **C_C** is the vector connecting the centroid of the $\{M(\mu\text{-}OH)\}_2$ core on one plane to that in the second plane in the stack. The use of these simple parameters gives an approach to analyze the distance and the degree of overlap for two molecules in the packing.

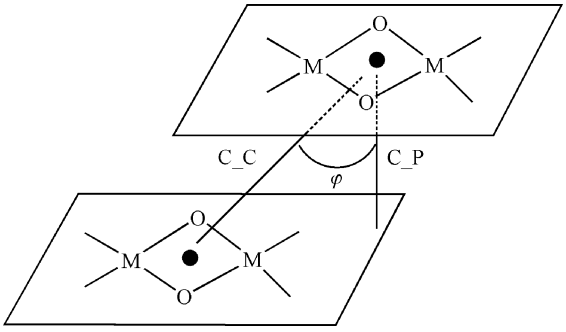

Figure 4. Relative positions of stacked molecules, C_P: centroid–plane distance; C_C: centroid–centroid distance; ϕ: deviation angle.

The results of the analysis covering only planar molecules and using the above parameters are summarized in Table 2. Two palladium (MARCUD and DEGKUW), three platinum (SUQQOK, MARDAK, and NIYHIM), and two copper complexes (QAFTIB and DPCUCL10) were retrieved from the CSD. Distances between planes in stacked molecules show a narrow range in spite of remarkable differences in ligands, counterions, or solvents in the crystal structure. As can be seen in Table 2, centroid–plane distances range between 3.17 and 3.48 Å, with a mean value of 3.33 Å. A certain deviation angle ϕ results as a consequence of the fact that stacking does not have a perfect face-to-face alignment of the atoms but an offset or slipped packing. Some degree of overlap can be expected even in structures having a centroid–centroid distance around 10 Å ($\phi \approx 70°$), as in DPCUL10. It is worth noting that reference codes MARCUD-MARDAK and DEGKUW-NIYHIM stand for couples corresponding to analogous complexes of palladium and platinum, which show similar packing with close values for C_P distance and ϕ angle (Table 2). In some cases a molecule stacks between two other molecules to which it is related by different distances and degrees of overlap.

Table 2. Relative positions of stacked molecules.

Reference code	C_P distance /Å	ϕ /°
SUQQOK	3.389	61.6
MARCUD	3.297	62.1
MARDAK	3.291	62.1
DEGKUW01	3.168, 3.451	52.3, 19.6
NIYHIM	3.211, 3.420	51.9, 19.8
QAFTIB	3.446	68.5
DPCUL10	3.297, 3.317	58.0, 71.4
Complex **1**	3.174	7.4
Complex **2**	3.478	20.7

Another unprecedented feature observed in the parallel orientation of molecules of complex **1** forming "trimers" is that it exhibits one of the closest centroid–plane distances together with, by far, the smallest ϕ deviation angle within all examples collected in Table 2. This indicates a very high degree of overlap, as justified in the theoretical section. Such an almost eclipsed overlap is neither frequent nor a favored manner of stacking.[26]

Theoretical Results

Quantum chemical calculations at the DFT level of theory were performed in order to grasp the unusual packing features in **1**, that is: (i) the preference of **1** for packing as three stacked parallel molecules, $\mathbf{1}_3$, and (ii) the interaction(s) responsible for a nearly eclipsed face-to-face stacking inside those "trimers".

First of all, we studied the model system **3** (Scheme 2), featuring the same $\{Pd(\mu\text{-}OH)(C\text{^}N)\}_2$ core as **1**, but lacking arene and heteroarene – phenyl and pyridyl – rings fused to the azapalladacycle that could give rise to π–π stacking interactions. Monomeric species **3** can exist as *cis* and *trans* isomers. Indeed, both types of palladacycles have been previously reported.[27] For the sake of simplicity, both types of monomeric structures are presented as simplified ball-and-stick sketches as shown in Scheme 2.

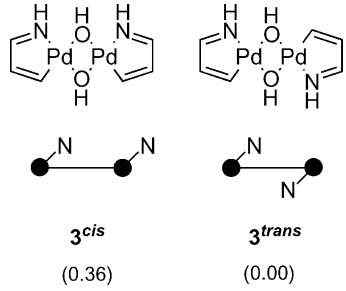

Scheme 2. Model monomers and their relative energies in kcal mol^{-1} (in parentheses).

None of these compounds has a planar structure. We have found that both of them are folded around the virtual O···O axis in their most stable conformations. The variation of the energy with the folding angle, calculated as the supplementary of the dihedral angle Pd–O–O–Pd, is represented in Figure 5. The most stable monomer **3** has the

trans configuration and a folding angle of 25.7°, whereby the planar conformation is a transition state between two such minima ($\tilde{\nu}$ = –14.1 cm^{-1}) representing an interconversion barrier of only 0.11 kcal mol^{-1} in the potential energy hypersurface. The absolute minimum for the *cis* isomer features a structure in which the two hydroxy groups are *trans* to each other and which is reached when the molecule is folded 29.7° as the chelate ring planes approach the hydroxy H atom which is further away from the nitrogen donor atoms. This structure is only 0.36 kcal mol^{-1} higher in energy than the *trans* diastereomer. The relative spatial orientation of the hydroxy group closest to the N atoms seems to be less energy-determining: there is only a small destabilization when it is oriented *cis* relative to the other one, especially in the proximity of the absolute minimum.

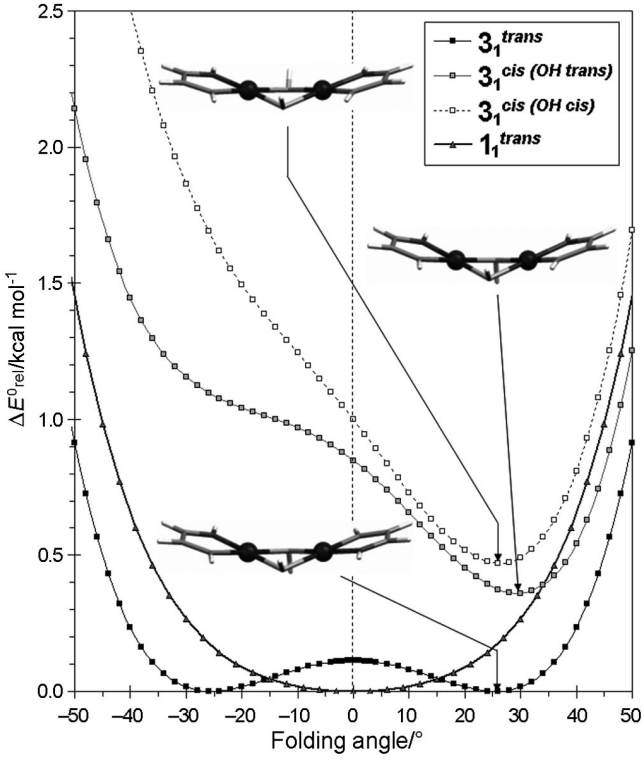

Figure 5. Influence of folding around the O–O axis (see text) on the calculated (method A) relative energy of monomeric models $\mathbf{3_1}$ and compound $\mathbf{1_1}$.

The observed preference for folding around the O–O axis in $\mathbf{3_1}^{trans}$ can be mainly attributed to the stabilization of HOMO-3 caused by Pd···Pd′ bonding interactions through d_{z^2}-type (*z* stands for the axis perpendicular to the mean plane) metal-centered atomic orbitals (AO) (Figure 6), as well as the increase of overlap between d_{xz}- and $d_{x^2-y^2}$-type (*x* stands for the axis containing the Pd atoms) orbitals at the Pd atom and p-type AO at the O atoms, causing the stabilization of HOMO, HOMO-4, HOMO-6, HOMO-7, and HOMO-9 (see Supporting Information).

Moving one step further, all model monomers $\mathbf{3_1}$ have at their outer (convex) surface two hydroxy groups oriented in such a way that could act simultaneously as hydrogen donor and/or acceptor towards a suitable complementary second

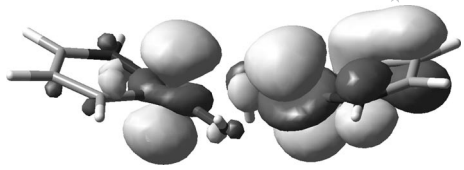

Figure 6. Calculated HOMO-3 (0.030 isovalue) in $\mathbf{3_1}^{trans}$.

monomeric unit $\mathbf{3_1}$ giving rise to a dimeric molecule $\mathbf{3_2}$. In the example shown in Figure 7, the recognition process between two units of self-complementary $\mathbf{3_1}^{trans}$ leading to dimer $\mathbf{3_2}^{t-th}$ is represented in the following way: both precursor molecules are displayed as electrostatic potential (from –0.1, white, to +0.1 a.u., black) mapped onto their respective electron density isosurfaces (0.0075 isovalue).

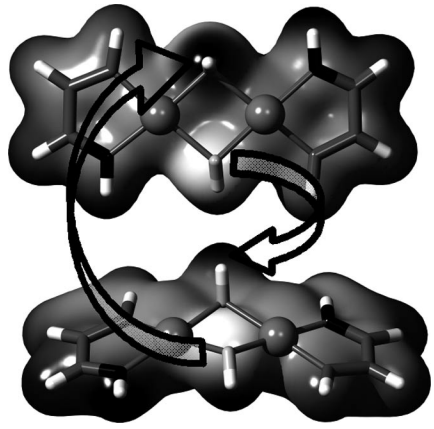

Figure 7. Electrostatic potential mapped onto an electron density isosurface (see text) for two molecules of $\mathbf{3_1}^{trans}$ showing the formation of two hydrogen bonds.

When two molecules of monomer **3** approach each other to form a dimer $\mathbf{3_2}$, five different diastereomeric topologies can result, which are sketched in Scheme 3. Two of them come from two *cis* monomers being assembled in an *erythro* (eclipsed) or *threo* (alternating) fashion ($\mathbf{3_2}^{c-er}$ and $\mathbf{3_2}^{c-th}$), two others from the same types of assemblies between *trans* monomers ($\mathbf{3_2}^{t-er}$ and $\mathbf{3_2}^{t-th}$), and a fifth topology results from the combination of a *cis* and a *trans* monomer ($\mathbf{3_2}^{c-t}$).

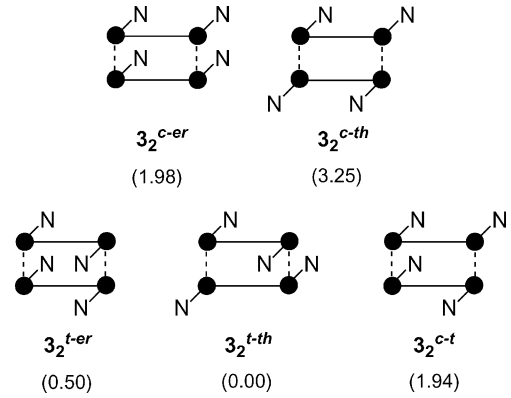

Scheme 3. Possible topologies for dimer $\mathbf{3_2}$ and their relative energies in kcal mol^{-1} in parentheses.

The most stable model dimer $\mathbf{3_2}$ is the *trans-threo* diastereomer, having overall C_2 symmetry (Figure 8a), whose formation from the most stable $\mathbf{3_1}^{trans}$ monomer is energetically favored (Table 3). Every subunit is slightly more folded (33.2°) than the precursor $\mathbf{3_1}^{trans}$. We have used the Bader's AIM (Atoms-In-Molecules) methodology[28] to perform a topological analysis of the electronic charge density $\rho(r)$. Besides the obvious ring critical points (3,+1) approximately at the centers of the four five-membered and two four-membered rings and one cage critical point (3,+3) roughly at the molecular center, we have found two pairs of different significant bond critical points (BCPs), also called (3,–1) critical points. Two of them are equivalent by symmetry and correspond to genuine strong hydrogen bridge bonds between hydroxy groups of different monomeric units. The other two BCPs lie halfway the bond path connecting every pair of Pd atoms that belong to different monomeric units and are indicative of stabilizing interactions between Pd atoms, which are situated at almost contact distance. Figure 8b displays the electrostatic potential (from –0.1, in white, to +0.1 au, in black) mapped onto an electron density isosurface whose isovalue (0.0075) has been chosen so as to show the higher electron density in the spatial region within the shorter and stronger Pd1–Pd1′ bond path when compared to the Pd2–Pd2′ one. Both the higher electron density at the BCP and the higher bond order, as measured by Wiberg's bond index (WBI), point to a greater relevance of hydrogen bonds in holding together the dimeric assembly, and consequently, to the only weak supplementary binding role of the Pd···Pd bonds.

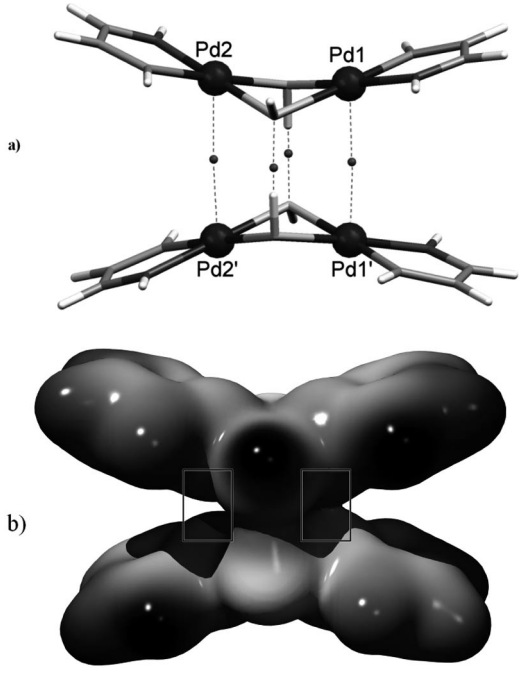

Figure 8. Calculated (method A) structure for model dimer $\mathbf{3_2}^{t-th}$. (a) Capped-stick representation: N atoms are highlighted in dark gray, and small spheres represent BCPs (the corresponding bond paths are sketched as dashed lines). (b) Electrostatic potential mapped onto an electron density isosurface (see text).

Furthermore, analysis of the MO diagram of $\mathbf{3_2}^{t-th}$ reveals two prominent features. In addition to those low lying MOs related with the hydrogen bridge bonding between monomeric subunits (see the Supporting Information), HOMO-6 and HOMO-9 (Figure 9, bottom) correspond to the two bonding Pd···Pd overlapping interactions involving d_{z^2}-type AO, and the two pairs are out-of-phase and in-

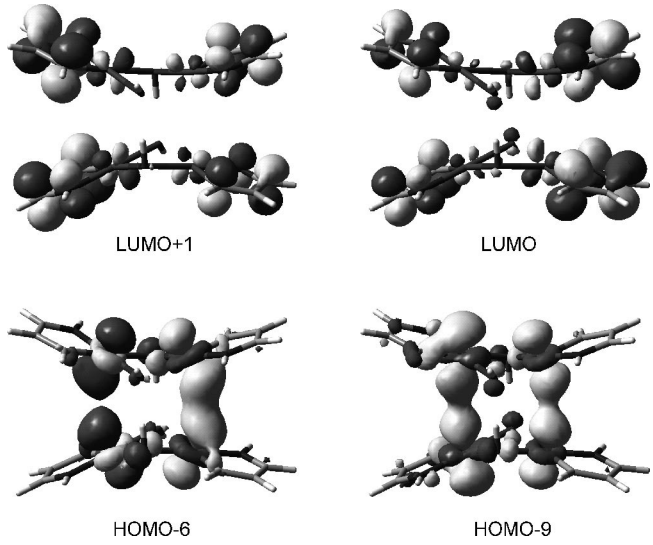

Figure 9. Relevant calculated MOs (0.030 isovalue) for model dimer $\mathbf{3_2}^{t-th}$.

Table 3. Relevant calculated (method A) parameters related to the interaction between monomeric subunits in compounds $\mathbf{1}_n$ and model systems $\mathbf{3}_n$, $\mathbf{4}_n$, $\mathbf{5}_n$, and $(H_2O)_n$ (n = 2, 3).

	$\mathbf{1_2}$	$\mathbf{1_3}$	$\mathbf{3_2}$	$\mathbf{3_3}$	$\mathbf{4_2}$	$\mathbf{4_3}$	$\mathbf{5_2}$	$\mathbf{5_3}$	$(H_2O)_2$	$(H_2O)_3$[a]
Growth energy[b]	–5.90	–0.34	–7.19	–0.58	2.40	3.01	–11.87	–3.60	–5.03	–5.90
Folding angle /°	24.9, 24.8	32.0, 0.0	33.2	33.8, 0.0						
Angle Pd–Pd–Pd /°		164.4		173.4		180.0		149.8		
$d_{OH\cdots O}$ /Å	1.884, 1.887	1.970, 2.105	1.867	1.973, 2.042					1.902	1.878
$WBI_{OH\cdots O} \times 10^{-2}$	5.2, 5.2	4.3, 2.4	5.6	4.2, 3.0					4.7	6.0
$\rho(r_c)$[c]	4.39, 4.36	3.67, 2.52	4.60	3.67, 2.91					4.27	4.54
$\nabla^2\rho(r_c)$[d]	4.07, 4.04	3.37, 2.55	4.20	1.24, 3.37					3.87	4.11
$d_{Pd\cdots Pd'}$ /Å	3.548, 3.554	3.432, 3.452	3.643, 3.871	3.383, 3.429	3.430	3.542	3.217	3.305		
$WBI_{Pd\cdots Pd'} \times 10^{-2}$	1.5, 1.5	1.8, 1.8	1.5, 1.1	2.0, 1.8	1.65	1.4	2.0	2.1		
$\rho(r_c)$[c]	1.45, 1.43	1.79, 1.74	1.22, 0.80	1.94, 1.76	1.76	1.47	2.62	2.24		
$\nabla^2\rho(r_c)$[d]	0.91, 0.91	1.14, 1.11	0.75, 0.49	1.24, 1.14	1.15	0.94	1.72	1.44		

[a] Average values;. [b] In kcal mol^{-1}. [c] In e Å$^{-3} \times 10^3$. [d] In e Å$^{-5} \times 10^3$.

phase, respectively. On the other hand, it is worth noting that LUMO+1 and LUMO (Figure 9, top) consist of combinations of (*C^N*)-ligand-centered AO with bonding character with respect to the interaction between the almost eclipsed five-membered palladacycles belonging to different monomeric subunits. Their very low population (formally unoccupied orbitals) excludes any favorable π–π stacking between the unsaturated organic residues, therefore explaining the divergent arrangement found.[29] Supporting Information contains details of the evolution of the MO diagram of $\mathbf{3_1}^{trans}$ upon interaction of two molecules to form $\mathbf{3_2}^{t-th}$.

The next step in increasing the molecular dimensionality would require the association of one dimer $\mathbf{3_2}$ with the convex molecular face of the appropriate monomer $\mathbf{3_1}$ having complementary hydrogen donor and/or acceptor sites at the hydroxido bridging ligands. As shown below, the subunit involved in the interacting molecular face of dimer $\mathbf{3_2}$ must experience a planarization. Among all possible resulting topologies let us consider only those three (Scheme 4) displaying the *Ci* symmetry found in the crystallographic analysis of compound **1**.

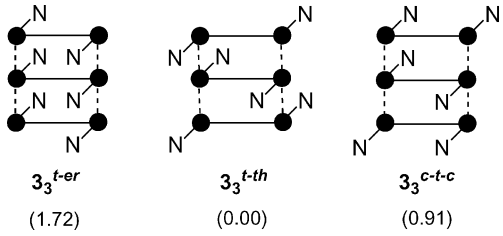

Scheme 4. Possible centrosymmetric topologies for trimer $\mathbf{3_3}$ and their relative energies in kcal mol^{-1} in parentheses.

Again the *trans-threo* diastereomer (Figure 10) is the most stable topology, and its formation from $\mathbf{3_2}^{t-th}$ and $\mathbf{3_1}^{trans}$ has been found to be scarcely favorable in terms of energy. Once the *cis-trans-cis* topology is ruled out because of its precedence from two chemically different species, the small difference of 1.69 kcal mol^{-1} between the *trans-threo* and *trans-erythro* trimers $\mathbf{3_3}$ is of great importance, because there is a crystallographic ambiguity in the crystal structure of **1**, in that it is not possible to directly discriminate between the *threo* and *erythro* diastereomers as a result of the similar scattering factors of carbon and nitrogen. The parameters characterizing the interactions that hold together the trimeric assembly are listed in Table 3. It is worthwhile to underline that the divergence angle between the central planar unit and one of the outer ones in $\mathbf{3_3}^{t-th}$ is much smaller (average value: 16.9°) than that observed for the most stable dimer $\mathbf{3_2}^{t-th}$ (average value: 33.2°). This could be due to the simultaneous effect of weaker –longer– hydrogen bonds that move further away the central O–O molecular hinges, and stronger –shorter– Pd···Pd contacts.

A last important conclusion that can be drawn from the study of model systems **3** is that, at the working level of theory, we have not been able to find any minimum corresponding to a hypothetical tetrameric derivative $\mathbf{3_4}$ upon interaction of either two units of dimer $\mathbf{3_2}$ or one trimer

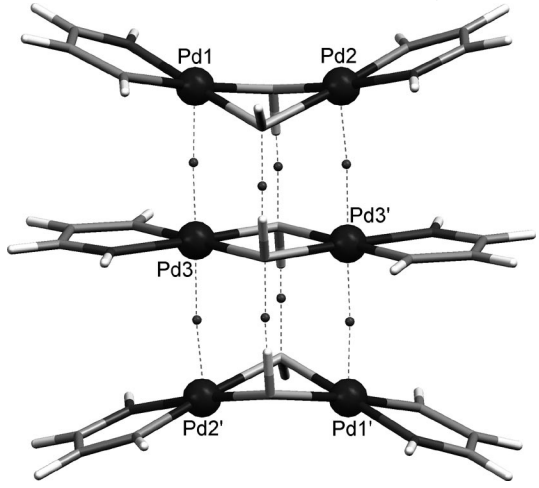

Figure 10. Calculated (method A) structure for model trimer $\mathbf{3_3}^{t-th}$ in capped-stick representation. N atoms are highlighted in dark gray. Small spheres represent BCPs, and the corresponding bond paths are sketched as dashed lines.

$\mathbf{3_3}$ with a monomer $\mathbf{3_1}$. This would explain the preferential formation of trimeric units as energetically most favored species in the solid-state crystalline structure of **1**.

When moving to the real systems bis[(μ^2-hydroxido)-(2-phenylpyridyl)palladium(II)] (**1**), we assumed that the most stable topologies $\mathbf{1_1}^{trans}$, $\mathbf{1_2}^{t-th}$, and $\mathbf{1_3}^{t-th}$ were kept for the monomeric, dimeric, and trimeric species, respectively, as in the previously studied model compounds. For the monomer $\mathbf{1_1}^{trans}$ we have found, however, a subtle difference: in this case the absolute minimum (Figure 11) corresponds to a centrosymmetric planar conformation (see the conformational analysis in Figure 5). A relatively weak hydrogen bond between the hydroxy O atom and the *ortho* H atom at the pyridine ring, ($d_{H\cdots O}$ = 2.558 Å, WBI 0.008), evidenced by the location of the corresponding BCP [$\rho(r_c)$ = 1.293×10^{-3} e Å^{-3}; $\nabla^2\rho(r_c)$ = 1.361×10^{-3} e Å^{-5}], may help in fixing this planar structure.[30]

The increase in the molecular dimensionality from monomer $\mathbf{1_1}^{trans}$ to dimer $\mathbf{1_2}^{t-th}$ and from the latter to trimer $\mathbf{1_3}^{t-th}$ is accomplished with gains in stability that are comparatively smaller than those computed for model systems **3** (Table 3). The differences in growth energy could be tentatively ascribed to repulsive interactions between pairs of aromatic ligands, comprising Pauli repulsion together with repulsive quadrupole–quadrupole forces, in spite of the fact that additional stabilizing interactions of the π–π stacking type could be expected to occur. Thus, in $\mathbf{1_2}^{t-th}$ two additional BCPs are observed at approximately halfway in between the C atoms belonging to different phenylpyridyl ligands on Pd1 and Pd1′ ($d_{C\cdots C}$ = 4.223 and 4.244 Å) and they have rather low electron density.[31] Analogously, these interactions are observed in trimer $\mathbf{1_3}^{t-th}$ at C···C contact distances between aromatic rings ($d_{C\cdots C}$ = 3.897 and 4.041 Å) that fall within the upper range for π–π stacking interactions. The weak bonding character is also underlined by the rather low electron density found at the corresponding BCPs.[31] The labile character of these π–π interactions

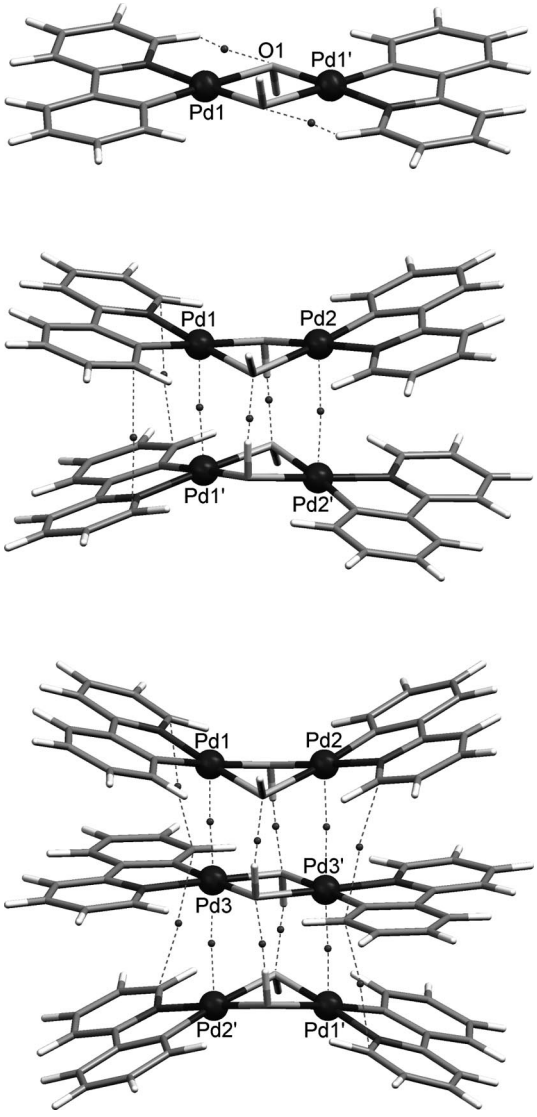

Figure 11. Calculated structures for monomer $\mathbf{1}_1^{trans}$ (top), dimer $\mathbf{1}_2^{t-th}$ (middle), and trimer $\mathbf{1}_3^{t-th}$ (bottom) in capped-stick representation. N atoms are highlighted in dark gray. Small spheres represent BCPs, and the corresponding bond paths are sketched as dashed lines.

is mainly due to the divergent arrangement of aromatic planes, which, in turn, is caused, as mentioned before, by a geometric compromise between the short O···HO central hydrogen bonds and the comparatively large pivotal Pd···Pd bonds.

Interactions between aromatic groups continue being among the most important but least understood of the noncovalent interactions. The simplest theory of dispersion predicts that it is proportional to the product of the polarizabilities of the two subsystems, and it is therefore particularly strong for groups with high polarizability, like π systems. It is straightforward to show that Hartree–Fock theory, and local and semilocal density functional theory (DFT) cannot describe genuine dispersion;[32] but, on the other hand, the simplest configuration-based electron-correlation theory, second-order Møller–Plesset theory (MP2), which approximately accounts for uncoupled two-body electron correlations, seriously overestimates the dispersion force at the basis set limit.[33] One way to improve upon the MP2 model of electron correlation is to include the coupling between electron pairs by use of the coupled-cluster theory; good results have been obtained with the *C*oupled-*C*luster with *S*ingle and *D*ouble and perturbative *T*riple excitations [CCSD(T)] method,[34] the so-called "gold standard" of quantum chemistry, also in conjunction with large basis sets and extrapolations to the complete basis set (CBS) limit,[35] but at a prohibitive computational cost for medium sized systems. Therefore we assume that even if our DFT-based level of theory reasonably accounts for the overall structure of $\mathbf{1}_3$, it is not appropriate for describing such subtle stacking interactions.

In summary, all central hydrogen bonds reported herein compare with that computed for the water dimer (H–O–H···OH_2) and trimer at the same level of theory (Table 3), not only in length but also in electron density at the BCP, the relatively large positive $\nabla^2\rho(r_c)$ value being usually diagnostic for the ionic character of the bonds.[36] We have found that the strength of the aforementioned hydrogen bonds decreases in the following order: dimers ($\mathbf{3}_2 > \mathbf{1}_2$) > water dimer > trimers ($\mathbf{3}_3 > \mathbf{1}_3$). Also there is a remarkable general agreement between the theoretically calculated structure for $\mathbf{1}_3$ and the experimentally obtained one. At the working level of theory (method A), chosen as a reasonable compromise between computational cost and accuracy (see below), the hydrogen bonds between monomeric units are slightly overestimated, giving rise to shorter interunit O···O distances (2.893 and 3.068 Å) than those found in the crystal structure (3.168 and 3.198 Å) reported herein. The same holds for the interaction between Pd atoms belonging to the same subunit (calcd. 3.084 and 3.200 Å; experimental 3.149 and 3.208 Å).

In order to allow a more comprehensive analysis of the Pd···Pd interaction between adjacent monomeric subunits, additional model systems where no internal hydrogen bonds can be formed, such as the dimers of compounds **4** and **5** (Scheme 5), were also considered. The Pd···Pd bond strength increases in roughly the opposite order to the hydrogen bond within the calculated structures: dimers ($\mathbf{3}_2 < \mathbf{1}_2$) < trimers ($\mathbf{1}_3 < \mathbf{3}_3$) ≤ non-hydrogen-bonded dimers ($\mathbf{4}_2 < \mathbf{5}_2$). These calculated Pd···Pd interactions were somehow underestimated when compared to the experimental ones (experimental Pd···Pd distances 3.161 and 3.255 Å), therefore leading to higher folding of the outer subunits (experimental 1.4°) which, in turn, increases the contact distances between heavy atoms in the aromatic phenylpyridyl ligands.

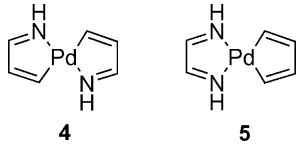

Scheme 5. Model non-hydrogen-bond-forming monomers.

With the aim of overcoming these subtle structural discrepancies, a more extensive basis set (method B: aug6-311G**/StRSCecp) was tested for all three model compounds $\mathbf{3_1}^{trans}$, $\mathbf{3_2}$, and $\mathbf{3_3}$, whereby only small improvements were achieved[37] for such an increase in computational cost.

Conclusions

Data retrieved from the CSD revealed that the most frequent conformation for the $\{M(\mu\text{-}O)\}_2$ core in di-(μ-OH) square-planar complexes of group 10 metals, is the planar one, and they usually stack in a parallel mode with distances between molecular planes in a narrow range of 3.2–3.4 Å. A DFT study of $[Pd(\mu\text{-}OH)(C\text{^}N)]_2$ (C^N = 2-phenylpyridyl) shows that a centrosymmetric planar conformation is the most stable arrangement partially as a result of a relatively weak hydrogen bond between the hydroxy O atom and the *ortho* H atom at the pyridine ring. This complex stacks in the solid state to form "trimers". DFT reveals that *threo* (alternating) *trans* orientation is the favorable one, which helps to unravel a crystallographic ambiguity due to the similarity between carbon and nitrogen atoms. Quantum chemical calculations also reveal that the stability in model "trimers" $\mathbf{3_3}$ is due to hydrogen bonds between OH groups and Pd···Pd interactions, whereas in $[Pd(\mu\text{-}OH)(C\text{^}N)]_2$ (C^N = 2-phenylpyridyl) complexes additional π–π stacking-type interactions are observed.

Experimental Section

Crystal Synthesis of $[Pd(\mu\text{-}OH)(C\text{^}N)]_2$ (1) {C^N = 2-(2-Pyridyl)-phenyl}: The complex was obtained by treating a solution of $[\{Pd(\mu\text{-}OOCMe)(phpy)\}_2]$ (0.500 mmol) in acetone (10 mL) with an aqueous solution of NBu_4OH (20%, 1.100 mmol). After 1 h of stirring at ambient temperature, a yellow solid was obtained, and the resulting suspension was then concentrated to one-fifth of the initial volume. Addition of water completed the precipitation of the complex, which was subsequently filtered off, then washed with water and hexane, and finally air-dried (yield, 90%).

Crystal Synthesis of $[Pd(\mu\text{-}OH)(C\text{^}N)]_2$ (2) (C^N = 7,8-Benzoquinolin-10-yl): The complex was obtained by treating a solution of $[\{Pd(\mu\text{-}OOCMe)(Bzq)\}_2]$ (Bzq = 7,8-benzoquinolyl), (0.500 mmol) in acetone (10 mL) with an aqueous solution of NBu_4OH (20%, 1.100 mmol). After 4 h of stirring at room temperature, a yellow solid was obtained, and the resulting suspension was then concentrated to one-fifth of the initial volume. Addition of water completed the precipitation of the complex, which was filtered off, washed with water, and air-dried (yield, 88%).

X-ray Diffraction: The X ray powder diffraction patterns were recorded by using a Philips X′PERT *θ*/*2θ* diffractometer with strictly monochromatic Cu-$K_{\alpha 1}$ radiation, 1.540598 Å, [Ge (111) primary monochromator] and an X′Celerator detector. Data were recorded between 5 and 100°, in the continuous scanning mode with a scan rate of 0.355° min^{-1}. Table 4 gives the most representative crystallographic parameters. CCDC-684985 (for **1**) and -684986 (for **2**) contain the supplementary crystallographic data for this paper. These data can be obtained free of charge from The Cambridge Crystallographic Data Centre via www.ccdc.cam.ac.uk/data_request/cif.

Table 4. Experimental crystallographic data.

Crystal data	Complex **1**	Complex **2**
Chemical formula	$C_{22}H_{18}N_2O_2Pd_2$	$C_{26}H_{18}N_2O_2Pd_2$
Formula mass	555.2	603.2
Cell setting	monoclinic	monoclinic
Space group	$P2_1/n$	$P2_1/n$
Temperature /K	298	298
a /Å	15.9720(6)	15.2268(8)
b /Å	16.1689(7)	3.71841(17)
c /Å	10.9567(4)	17.7256(10)
β /°	92.137(2)	92.497(3)
V /Å^3	2827.60(19)	1002.66(9)
Z	6	2
D_x /Mg m^{-3}	1.956	1.998
Radiation type /K	Cu-$K_{\alpha 1}$	Cu-$K_{\alpha 1}$
Specimen color and form	yellow powder	yellow powder
Specimen size	micrometric	micrometric
Data collection		
Diffractometer	Philips X′PERT	Philips X′PERT
Data collection method	continuous scan	continuous scan
2*θ* /°	5–100	5–100
Refinement		
Refinement on	intensity	intensity
R factors and goodness of fit	R_p = 0.082, R_{wp} = 0.112, $R_{exp.}$ = 0.034, R_B = 0.066, S = 3.25	R_p = 0.068, R_{wp} = 0.093, $R_{exp.}$ = 0.033, R_B = 0.038, S = 2.85
Wavelength of incident radiation /Å	1.54059	1.54059
Excluded region(s)	none	none
Profile function	pseudo-Voigt	pseudo-Voigt
No. of parameters	94	85
Hydrogen-atom treatment	constrained to parent site	constrained to parent site

Cambridge Structural Database Survey: The Cambridge Structural Database[38] (CSD) V. 5.29 (November 2007) was searched for: (a) all the structures containing the $\{M(\mu\text{-}OH)\}_2$ core (M = Ni, Pd, Pt) and (b) dinuclear di-(μ-OH) complexes showing a planar conformation. The query was filtered so that structures without errors and without disorder were retrieved.

Computational Details: Calculated geometries for all studied complexes were fully optimized without symmetry constraints in the gas phase with tight convergence criteria by using the Gaussian 03[39] package at the DFT level of theory, with the B3LYP functional.[40] Unless otherwise stated, the 6-31G* basis set was employed for all atoms, but with the addition of diffuse functions for N and O (denoted as aug6-31G*), except for Pd, for which the SDD basis set with ECP (effective core potential) was used (method A). From these gas-phase optimized geometries, all reported data were obtained by means of single-point (SP) calculations. The reduced 6-31G*/SDDecp basis set (without diffuse functions) was used to perform the Natural Bond Orbital (NBO) population analysis. Bond orders were characterized by Wiberg's bond index[41] (WBI) and calculated with the NBO method as the sum of squares of the off-diagonal density matrix elements between atoms. Reported total electronic energies are uncorrected for the ZPVE (zero point vibrational energy). The growth energies are evaluated by using total (uncorrected) electronic energies for every species involved in the sequential growing process of an *n*th order oligomer ($M_{n-1} + M \rightarrow M_n$) and correcting the basis set superposition error (BSSE) by means of the counterpoise approach.[42] The topological analysis of the electronic charge density was conducted by means

of Bader's AIM (Atoms-In-Molecules) methodology with the AIM2000 software.[43] Also, for comparative purposes and for convenience of presentation, the highest aug6-311G** (with diffuse functions on N and O) basis set was employed, together with the Stuttgart relativistic small-core basis set (StRSC) with ECP[44] for Pd (method B). In such cases, the AIM analyses were carried out at the same level, whereas the reduced 6-311G**/StRSCecp basis set was employed for the NBO SP calculations.

Molecular graphics images in Figure 7 and Figure 8b were produced with the UCSF Chimera package[45] from the Resource for Biocomputing, Visualization, and Informatics at the University of California, San Francisco (supported by NIH P41 RR-01081).

Supporting Information (see footnote on the first page of this article): Full MO diagram evolution upon folding of $\mathbf{3_1}^{trans}$, from the planar transition state to the folded absolute minimum, and upon dimerization of the latter to afford $\mathbf{3_2}^{t-th}$. Cartesian coordinates and energies for all calculated compounds.

Acknowledgments

A. E. gratefully acknowledges the financial support from Fundación Séneca (Agencia de Ciencia y Tecnología de la Región de Murcia) projects 02970/PI/05 and 04509/GERM/06 (Programa de Ayudas a Grupos de Excelencia de la Región de Murcia, Plan Regional de Ciencia y Tecnología 2007/2010).

[1] K. A. Hirsch, S. R. Wilson, J. S. Moore, *Chem. Eur. J.* **1997**, *3*, 765–771.
[2] G. Filippini, A. Gavezotti, *Acta Crystallogr., Sect. B* **1993**, *49*, 868–880.
[3] A. Gavezotti, G. Filippini, *J. Am. Chem. Soc.* **1996**, *118*, 7153–7157.
[4] S. Kitagawa, M. Kondo, *Bull. Chem. Soc. Jpn.* **1998**, *71*, 1739–1753.
[5] G. Guilera, J. W. Steed, *Chem. Commun.* **1999**, 1563–1564.
[6] C. Janiak, *Angew. Chem. Int. Ed. Engl.* **1997**, *36*, 1431–1434.
[7] C. A. Hunter, J. K. M. Sanders, *J. Am. Chem. Soc.* **1990**, *112*, 5525–5534.
[8] R. Büchner, C. T. Cunningham, J. S. Field, R. J. Haines, D. R. McMillin, G. C. Summerton, *J. Chem. Soc., Dalton Trans.* **1999**, 711–717.
[9] M. Kato, C. Kosuge, K. Morii, J. S. Ahn, H. Kitagawa, T. Mitani, M. Matsushita, T. Kato, S. Yano, M. Kimura, *Inorg. Chem.* **1999**, *38*, 1638–1641.
[10] L. Hao, R. J. Lacchicotte, H. J. Gysling, R. Eisenberg, *Inorg. Chem.* **1999**, *38*, 4616–4617.
[11] N. W. Alcock, P. R. Barker, J. M. Haider, M. J. Hannon, C. L. Painting, Z. Pikramenou, E. A. Plummer, K. Rissanen, P. Saarenketo, *J. Chem. Soc., Dalton Trans.* **2000**, 1447–1461.
[12] R. A. Adrian, G. A. Broker, E. R. T. Tiekink, J. A. Walmsley, *Inorg. Chim. Acta* **2008**, *361*, 1261–1266.
[13] a) J. L. Serrano, I. J. S. Fairlamb, G. Sánchez, L. García, J. Pérez, J. Vives, G. López, C. M. Crawforth, R. J. K. Taylor, *Eur. J. Inorg. Chem.* **2004**, 2706–2715; b) J. Ruiz, V. Rodríguez, G. López, J. Casabó, E. Molins, C. Miravitlles, *Organometallics* **1999**, *18*, 1177–1184 and references cited therein; c) G. Sánchez, J. L. Serrano, J. García, G. López, J. Pérez, E. Molins, *Inorg. Chim. Acta* **1999**, *287*, 37–46; d) G. Sánchez, J. L. Serrano, J. Pérez, M. C. Ramírez de Arellano, G. López, E. Molins, *Inorg. Chim. Acta* **1999**, *295*, 136–145.
[14] T. Roisnel, J. Rodríguez-Carvajal, *Mater. Sci. Forum* **2001**, *118*, 378.
[15] J. Laugier, B. Bochu, *CHECKCELL*: a Software Performing Automatic Cell/Space Group Determination, Collaborative Computational Project, Number 14 (CCP14), Laboratory of Materials and Physical Engineering, School of Physics, University of Grenoble, France, **2000**.
[16] C. J. E. Kempster, H. Lipson, *Acta Crystallogr., Sect. B* **1972**, *28*, 3674–3674.
[17] A. Le Bail, H. Duroy, J. L. Fourquet, *Mater. Res. Bull.* **1988**, *23*, 447–452.
[18] J. Rodriguez-Carvajal, *FULLPROF*, V. 1.9c. LLB, CEA/Saclay, France, **2001**.
[19] J. Baldinozzi, J. F. Berar, *J. Appl. Crystallogr.* **1993**, *26*, 128–129.
[20] V. Favre-Nicolin, R. Cerný, *FOX*: a Program for ab initio Structure Solution from Powder Diffraction Data, Laboratory of Crystallography, University of Geneva, Switzerland, **2000**.
[21] A. March, *Z. Kristallogr.* **1932**, *81*, 285–297.
[22] W. A. Dollase, *J. Appl. Crystallogr.* **1986**, *19*, 267–272.
[23] M. C. Burla, R. Caliandro, M. Camalli, B. Carrozzini, G. L. Cascarano, L. De Caro, C. Giacovazzo, G. Polidori, R. Spagna, *J. Appl. Crystallogr.* **2005**, *38*, 381–388.
[24] J. Pérez, J. L. Serrano, J. M. Galiana, F. L. Cumbrera, A. L. Ortiz, G. Sánchez, J. García, *Acta Crystallogr., Sect. B* **2007**, *63*, 75–80.
[25] a) R. A. Adrian, R. E. Benson, L. M. Daniels, E. R. T. Tiekink, J. A. Walmsley, *Acta Crystallogr., Sect. E: Struct. Rep. Online* **2006**, *62*, m601–m603; b) A. D. Getty, K. I. Goldberg, *Organometallics* **2001**, *20*, 2545–2551; c) A. L. Spek, M. A. Zuideveld, P. W. N. M. van Leeuwen, Private communication, **2004**; d) C. Pisano, G. Consiglio, A. Sironi, M. Moret, *J. Chem. Soc., Chem. Commun.* **1991**, 421–423; e) A. Fujii, E. Hagiwara, M. Sodeoka, *J. Am. Chem. Soc.* **1999**, *121*, 5450–5458; f) V. V. Grushin, H. Alper, *Organometallics* **1993**, *12*, 1890–1901; g) S. Kannan, A. J. James, P. R. Sharp, *Polyhedron* **2000**, *19*, 155–163; h) R. D. Schnebeck, E. Freisinger, B. Lippert, *Eur. J. Inorg. Chem.* **2000**, 1193–1200; i) J. L. Serrano, I. J. S. Fairlamb, G. Sanchez, L. Garcia, J. Perez, J. Vives, G. Lopez, C. M. Crawforth, R. J. K. Taylor, *Eur. J. Inorg. Chem.* **2004**, 2706–2715; j) Jianke Liu, B. T. Heaton, J. A. Iggo, R. Whyman, J. F. Bickley, A. Steiner, *Chem. Eur. J.* **2006**, *12*, 4417–4430; k) M. Akita, T. Miyaji, N. Muroga, C. Mock-Knoblauch, W. Adam, S. Hikichi, Y. Moro-oka, *Inorg. Chem.* **2000**, *39*, 2096–2102; l) G. Lopez, J. Ruiz, G. Garcia, C. Vicente, J. Casabo, E. Molins, C. Miravitlles, *Inorg. Chem.* **1991**, *30*, 2605–2610; m) L. J. Ackerman, J. P. Sadighi, D. M. Kurtz, J. A. Labinger, J. E. Bercaw, *Organometallics* **2003**, *22*, 3884–3890; n) D. Nama, P. S. Pregosin, A. Albinati, S. Rizzato, *Organometallics* **2007**, *26*, 2111–2121; o) G. Pieri, M. Pasquali, P. Leoni, U. Englert, *J. Organomet. Chem.* **1995**, *491*, 27–30; p) W.-Z. Shen, D. Gupta, B. Lippert, *Inorg. Chem.* **2005**, *44*, 8249–8258.
[26] C. Janiak, *J. Chem. Soc., Dalton Trans.* **2000**, 3885–3896.
[27] J. Dupont, C. S. Consorti, J. Spencer, *Chem. Rev.* **2005**, *105*, 2527–2571.
[28] R. F. W. Bader, *Atoms in Molecules: A Quantum Theory*, Oxford University Press, Oxford, **1990**.
[29] Indeed, filling the LUMO of $\mathbf{3_2}^{t-th}$ with one electron, as would occur in a hypothetical, derived radical anion, approximates the five-membered chelate rings involving Pd1 and Pd1′ [$d_{Pd1-Pd1}$ = 3.182 Å; $WBI_{Pd1-Pd1}$ 0.007; $\rho(r_c)$= 2.803×10^{-3} e Å^{-3}; $\nabla^2\rho(r_c)$ = 1.748×10^{-3} e Å^{-5}] so as to let them become almost parallel and favor a strong π–π interaction, as evidenced by the bond critical point found between C atoms close to N atoms in both metallacycles [d_{C-C} = 3.292 Å; WBI_{C-C} 0.018; $\rho(r_c)$= 1.021×10^{-3} e Å^{-3}; $\nabla^2\rho(r_c)$ = 0.670×10^{-3} e Å^{-5}].
[30] For the analogous larger interaction with the *ortho* H atom at the phenyl ring ($d_{H\cdots O}$ = 2.664 Å, WBI 0.006), we have not found the corresponding BCP.
[31] For $\mathbf{1_2}^{t-th}$: $\rho(r_c)$= 1.71×10^{-4} and 1.65×10^{-4} e Å^{-3} and $\nabla^2\rho(r_c)$ = 1.50×10^{-4} and 1.46×10^{-4} e Å^{-5}. For $\mathbf{1_3}^{t-th}$: $\rho(r_c)$= 4.34×10^{-4} and 2.95×10^{-4} e Å^{-3}; with $\nabla^2\rho(r_c)$ = 3.50×10^{-4} and 2.43×10^{-4} e Å^{-5}.

[32] S. Kristyán, P. Pulay, *Chem. Phys. Lett.* **1994**, *229*, 175–180; E. R. Johnson, R. A. Wolkow, G. A. DiLabio, *Chem. Phys. Lett.* **2004**, *394*, 334–338.
[33] R. L. Jaffe, G. D. Smith, *J. Chem. Phys.* **1996**, *105*, 2780–2788; P. Hobza, H. L. Selzle, E. W. Schlag, *J. Phys. Chem.* **1996**, *100*, 18790–18794; S. Tsuzuki, T. Uchimaru, K. Matsumura, M. Mikami, K. Tanabe, *Chem. Phys. Lett.* **2000**, *319*, 547–554; S. Tsuzuki, H. P. Lüthi, *J. Chem. Phys.* **2001**, *114*, 3949–3957.
[34] K. Raghavachari, G. W. Trucks, J. A. Pople, *Chem. Phys. Lett.* **1989**, *157*, 479–483; B. W. Hopkins, G. S. Tschumper, *J. Phys. Chem. A* **2004**, *108*, 2941–2948.
[35] M. O. Sinnokrot, C. D. Sherrill, *J. Phys. Chem. A* **2006**, *110*, 10656–10668; T. Janowski, P. Pulay, *Chem. Phys. Lett.* **2007**, *447*, 27–32; E. C. Lee, D. Kim, P. Jurečka, P. Tarakkeshwar, P. Hobza, K. S. Kim, *J. Phys. Chem. A* **2007**, *111*, 3446–3457.
[36] W. Nakanishi, T. Nakamoto, S. Hayashi, T. Sasamori, N. Tokitoh, *Chem. Eur. J.* **2007**, *13*, 255–268 and references cited therein.
[37] Selected parameters for optimized (method B) model compounds. For $\mathbf{3_1}^{trans}$: folding angle 6.9°. For $\mathbf{3_2}^{t-th}$: ΔE_{growth} = –9.72 kcal mol^{-1}; folding angle 31.9°; $d_{OH\cdots O}$ = 1.895 Å, $WBI_{OH\cdots O}$ 0.035, $\rho(r_c)$= 4.153×10^{-3} e Å^{-3}, $\nabla^2\rho(r_c)$ = 4.219×10^{-3} e Å^{-5}, $d_{O(H)\cdots O}$ = 2.858 Å; $d_{Pd\cdots Pd'}$ = 3.639 and 3.847 Å, $WBI_{Pd\cdots Pd'}$ 0.014 and 0.011, $\rho(r_c)$= 1.221×10^{-3} and 8.303×10^{-4} e Å^{-3}, $\nabla^2\rho(r_c)$ = 7.573×10^{-4} and 5.124×10^{-4} e Å^{-5}. For $\mathbf{3_3}^{t-th}$: ΔE_{growth} = –3.96 kcal mol^{-1}; folding angle 33.1 and 0.0°; angle Pd–Pd–Pd 172.9°; $d_{OH\cdots O}$ = 2.016 and 2.082 Å, $WBI_{OH\cdots O}$ 0.023 and 0.015, $\rho(r_c)$= 3.250×10^{-3} and 2.545×10^{-3} e Å^{-3}, $\nabla^2\rho(r_c)$ = 3.308×10^{-3} and 2.822×10^{-3} e Å^{-5}, $d_{O(H)\cdots O}$ = 2.910 and 3.030 Å; $d_{Pd\cdots Pd'}$ = 3.409 and 3.450 Å, $WBI_{Pd\cdots Pd'}$ 0.019 and 0.017, $\rho(r_c)$ = 1.853×10^{-3} and 1.691×10^{-3} e Å^{-3}, $\nabla^2\rho(r_c)$ = 1.181×10^{-3} and 1.092×10^{-3} e Å^{-5}.
[38] F. H. Allen, *Acta Crystallogr., Sect. B* **2002**, *58*, 380–388.
[39] M. J. Frisch, G. W. Trucks, H. B. Schlegel, G. E. Scuseria, M. A. Robb, J. R. Cheeseman, J. A. Montgomery Jr, T. Vreven, K. N. Kudin, J. C. Burant, J. M. Millam, S. S. Iyengar, J. Tomasi, V. Barone, B. Mennucci, M. Cossi, G. Scalmani, N. Rega, G. A. Petersson, H. Nakatsuji, M. Hada, M. Ehara, K. Toyota, R. Fukuda, J. Hasegawa, M. Ishida, T. Nakajima, Y. Honda, O. Kitao, H. Nakai, M. Klene, X. Li, J. E. Knox, H. P. Hratchian, J. B. Cross, V. Bakken, C. Adamo, J. Jaramillo, R. Gomperts, R. E. Stratmann, O. Yazyev, A. J. Austin, R. Cammi, C. Pomelli, J. W. Ochterski, P. Y. Ayala, K. Morokuma, G. A. Voth, P. Salvador, J. J. Dannenberg, V. G. Zakrzewski, S. Dapprich, A. D. Daniels, M. C. Strain, O. Farkas, D. K. Malick, A. D. Rabuck, K. Raghavachari, J. B. Foresman, J. V. Ortiz, Q. Cui, A. G. Baboul, S. Clifford, J. Cioslowski, B. B. Stefanov, G. Liu, A. Liashenko, P. Piskorz, I. Komaromi, R. L. Martin, D. J. Fox, T. Keith, M. A. Al-Laham, C. Y. Peng, A. Nanayakkara, M. Challacombe, P. M. W. Gill, B. Johnson, W. Chen, M. W. Wong, C. Gonzalez, J. A. Pople, *Gaussian 03*, Revision B.03, Gaussian, Inc., Wallingford CT, **2004**.
[40] L. J. Bartolotti, K. Fluchick in *Reviews in Computational Chemistry, Vol. 7* (Eds.: K. B. Lipkowitz, D. B. Boyd), VCH Publishers, New York, **1996**, pp. 187–216.
[41] K. Wiberg, *Tetrahedron* **1968**, *24*, 1083–1096.
[42] S. F. Boys, F. Bernardi, *Mol. Phys.* **1970**, *19*, 553–566.
[43] *AIM2000* v. 2.0, designed by F. W. Biegler-König and J. Schönbohm, **2002**. Home page http://www.aim2000.de/; F. Biegler-König, J. Schönbohm, D. Bayles, *J. Comput. Chem.* **2001**, *22*, 545–559; F. Biegler-König, J. Schönbohm, *J. Comput. Chem.* **2002**, *23*, 1489–1494.
[44] The Stuttgart relativistic small-core basis set was obtained from the Extensible Computational Chemistry Environment Basis Set Database, Version 10/29/02, as developed and distributed by the Molecular Science Computing Facility, Environmental and Molecular Sciences Laboratory, which is part of the Pacific Northwest Laboratory, P. O. Box 999, Richland, Washington 99352, USA, and funded by the U. S. Department of Energy. The Pacific Northwest Laboratory is a multi-program laboratory operated by Battelle Memorial Institute for the U. S. Department of Energy under contract DE-AC06-76RLO 1830.
[45] E. F. Pettersen, T. D. Goddard, C. C. Huang, G. S. Couch, D. M. Greenblatt, E. C. Meng, T. E. Ferrin, *J. Comput. Chem.* **2004**, *25*, 1605–1612.

Received: April 15, 2008
Published Online: July 9, 2008

